JOURNAL OF COMPUTATIONAL PHYSICS 58, 300–335 (1985)

The Princeton Spectral Equilibrium Code: PSEC

K. M. LING AND S. C. JARDIN

Plasma Physics Laboratory, Princeton University, Princeton, New Jersey 08544

Received February 21, 1984; revised May 1, 1984

A fast computer code has been developed to calculate free-boundary solutions to the plasma equilibrium equation that are consistent with the currents in external coils and conductors. The free-boundary formulation is based on the minimization of a mean-square error ε while the fixed-boundary solution is based on a variational principle and spectral representation of the coordinates $x(\psi, \theta)$ and $z(\psi, \theta)$. Specific calculations using the Columbia University Torus II, the Poloidal Divertor Experiment (PDX), and the Tokamak Fusion Test Reactor (TFTR) geometries are performed.

I. INTRODUCTION

Numerical solutions of the equations describing toroidal plasma equilibrium continue to play a central role in the magnetic confinement thermonuclear fusion program. Experimentalists are increasingly using these solutions to interpret experimental data and to design new experiments. Theorists are using them as starting points for realistic stability, transport, orbit, and ray tracing calculations.

A recent development has shown that a spectral representation can be used effectively with a variational principle to obtain efficient equilibrium solutions if the shape of the plasma–vacuum interface is known [1]. The spectral method has been shown to be particularly useful for obtaining very rapid "approximate" solutions to the equilibrium equation in which only a few basis functions are retained, but the gross features of the solution are nevertheless calculated reasonably accurately. These approximate solutions are often adequate for experimental studies or for gross theoretical parametric studies.

In this paper the spectral variational method for finding numerical solutions to the plasma equilibrium equation is extended to the calculation of free-boundary solutions that are consistent with the currents in external coils and conductors [2]. This is naturally done by the minimization of a mean-square error ε which measures the deviation of the plasma–vacuum boundary from being an exact magnetic flux surface. The fixed-boundary variational principle gives a set of coupled second-order ordinary differential equations for the spectral amplitudes of the coordinates x and z once their boundary values are known. The minimization of ε yields a set of coupled algebraic equations which self-consistently determine the

0021-9991/85 $3.00

boundary spectral amplitudes. Thus one can envision an iteration scheme where at each free-boundary iteration step a fixed-boundary problem is solved.

In Section II, the mathematical formulation of both the fixed-boundary and free-boundary problems is given. The method of solution is described in Section III. Code verification and applications are given in Sections IV and V, and a summary is given in Section VI.

II. Mathematical Formulation

A. *Variational Principle for Fixed-Boundary Equilibrium*

In this section we state a variational principle which forms the basis for obtaining spectral solutions to the equilibrium equation in magnetic coordinates for a fixed shape plasma boundary. This formulation is augmented in Section D to provide a prescription for determining the location of the plasma boundary consistent with a set of external current-carrying coils.

In the cylindrical (x, ϕ, z) coordinates (Fig. 1) the magnetic field in an axisymmetric toroidal system can be written as

$$\vec{B} = B_0(\nabla\phi \times \nabla\chi + R_0\, g\, \nabla\phi), \tag{1}$$

where R_0 is a constant with dimensions of length, χ is the normalized poloidal flux function, $|\nabla\phi| = x^{-1}$, and $g = g(\chi)$ is the dimensionless toroidal field function. The overall constant B_0 is present in the coded implementation of this method but will be suppressed in the following discussion. To restore it, we merely multiply each

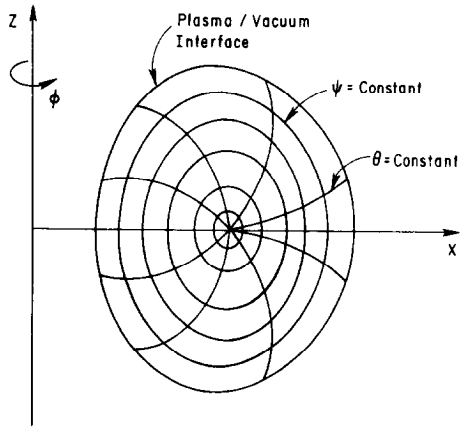

FIG. 1. Cylindrical coordinate system (x, ϕ, z) and flux coordinates (ψ, θ, ϕ). ψ is a flux label, θ a poloidal angle, and ϕ is the ignorable toroidal angle.

occurrence of χ and g in the paper by B_0. The magnitudes of the poloidal and toroidal magnetic fields are then given by

$$B_p^2 = |\nabla\chi|^2/x^2, \tag{2a}$$

$$B_T^2 = R_0^2 g^2/x^2. \tag{2b}$$

We define an "action integral" A

$$A = \int_V dx\, dz\, L(\chi, \chi_x, \chi_z; x), \tag{3}$$

where L is the Lagrangian density

$$L = x(B_P^2 - 2p - B_T^2). \tag{4}$$

Here $p = p(\chi)$ is the fluid pressure and the integration is over the entire plasma volume V. The functional dependence of L has been made explicit, with the subscripts denoting partial derivatives.

A variational principle [3, 4] has been given which states that A is stationary with respect to variations of χ for χ satisfying the equilibrium force balance (Grad–Shafranov) equation

$$\Delta^*\chi \equiv x^2\nabla\cdot(x^{-2}\nabla\chi) = -[p'x^2 + R_0^2 gg'] \tag{5}$$

subject to the constraint that the variations vanish on the boundary,

$$\delta\chi\,(\text{boundary}) = 0. \tag{6}$$

Here the prime superscript denotes $d/d\chi$. Conversely, it is readily verified that the Euler–Lagrange equation

$$\frac{\partial L}{\partial\chi} - \frac{\partial}{\partial x}\frac{\partial L}{\partial\chi_x} - \frac{\partial}{\partial z}\frac{\partial L}{\partial\chi_z} = 0 \tag{7}$$

gives back the Grad–Shafranov equation, Eq. (5).

Next consider a transformation from the cylindrical (x, ϕ, z) coordinates to the magnetic flux coordinates (ψ, θ, ϕ) where ψ is a flux surface label normalized such that $\psi = 0$ at the magnetic axis and $\psi = 1$ at the boundary, θ is a poloidal angle $(0 < \theta < 2\pi)$, and ϕ the ignorable toroidal angle with $|\nabla\phi|^2 = 1/x^2$ (Fig. 1). The directions $\nabla\psi$ and $\nabla\theta$ are not necessarily orthogonal to each other, but both $\nabla\psi$ and $\nabla\theta$ are orthogonal to $\nabla\phi$. The action integral A, Eq. (3), becomes

$$A = \int_0^1 \int_0^{2\pi} d\theta\, d\psi\, L(x, x_\psi, x_\theta, z_\psi, z_\theta, \chi, \chi_\psi; \psi, \theta). \tag{8}$$

Noting that $|\nabla\chi|^2 = \chi_\psi^2\,|\nabla\psi|^2 = \chi_\psi^2 x^2(x_\theta^2 + z_\theta^2)/J^2$, we find that the Lagrangian density L is given by

$$L = J[\chi_\psi^2(x_\theta^2 + z_\theta^2)/J^2 - 2p - R_0^2\, g^2/x^2], \tag{9}$$

where the Jacobian of the transformation J is given by

$$J \equiv [\nabla\psi \times \nabla\theta \cdot \nabla\phi]^{-1} = x(x_\psi z_\theta - z_\psi x_\theta). \tag{10}$$

The subscripts ψ and θ denote the partial derivatives with respect to ψ and θ, respectively. Before the coordinate transformation, $\chi = \chi(x, z)$ with x and z being the independent variables. After the transformation $\chi = \chi(\psi)$, $x = x(\psi, \theta)$, and $z = z(\psi, \theta)$ with ψ and θ being the independent variables. We note that at this point the poloidal angle θ is still arbitrary.

The equilibrium force balance equation in the flux coordinate system, i.e., the inverse Grad–Shafranov equation, is

$$G \equiv 2\chi_\psi \left\{ \frac{1}{J}\frac{\partial}{\partial\psi}[\chi_\psi(x_\theta^2 + z_\theta^2)/J] - \frac{1}{J}\frac{\partial}{\partial\theta}[\chi_\psi(x_\psi x_\theta + z_\psi z_\theta)/J] + p' + R_0^2\, gg'/x^2 \right\} = 0. \tag{11}$$

Since A is independent of the coordinate representation, it must be stationary with respect to variations in x and z. Indeed, if $G = 0$, A given by Eq. (8) is stationary with respect to variations in x or z subject to the fixed-boundary constraint δx (boundary) $= 0$ or δz (boundary) $= 0$. The Euler–Lagrange equations

$$\frac{\partial L}{\partial x} - \frac{\partial}{\partial\psi}\frac{\partial L}{\partial x_\psi} - \frac{\partial}{\partial\theta}\frac{\partial L}{\partial x_\theta} = 0 \tag{12a}$$

or

$$\frac{\partial}{\partial\psi}\frac{\partial L}{\partial z_\psi} + \frac{\partial}{\partial\theta}\frac{\partial L}{\partial z_\theta} = 0 \tag{12b}$$

will both reproduce Eq. (11).

B. *Spectral Representation*

The usefulness of the stated variational principle is that it allows us to expand the coordinate functions $x(\psi, \theta)$ and $z(\psi, \theta)$ in terms of a complete set of basis functions, and to vary their coefficients independently to obtain a set of defining equations for the amplitudes. When the series is truncated to a finite set of basis functions, the amplitudes obtained this way are "optimal" in the sense that they minimize the Lagrangian density, Eq. (9).

We find it convenient to let $x(\psi, \theta)$ and $z(\psi, \theta)$ have the following series expansion:

$$x(\psi, \theta) = x^{0c}(\psi) + \sqrt{\psi T}\, E(\psi) \cos\theta + \sum_{m=2}^{M} \psi^{(m-2)/2}[x^{mc}(\psi) \cos m\theta + x^{ms}(\psi) \sin m\theta], \tag{13a}$$

$$z(\psi, \theta) = z^{0c}(\psi) + \sqrt{\psi T}\, E^{-1}(\psi) \sin\theta + \sqrt{\psi}\, z^{1c}(\psi) \cos\theta + \sum_{m=2}^{M} \psi^{(m-2)/2}[\sigma_{a,m} x^{ms}(\psi) \cos m\theta + \sigma_{s,m} x^{mc}(\psi) \sin m\theta]. \tag{13b}$$

The scale factor T is introduced so that without loss of generality, the flux surface label ψ goes from 0 at the magnetic axis to 1 at the boundary. The constants $\sigma_{a,m}$ and $\sigma_{s,m}$ are independent of ψ and are usually set to $+1$ and -1, respectively. The ellipticity E here is different from the conventional definition of ellipticity ($E_{\text{conv}} = 1/E^2$). The factor $\psi^{(m-2)/2}$ is chosen to simplify the boundary conditions at the magnetic axis as is explained in Section C. The poloidal angle θ is specified implicitly by Eq. (13) since the same set of spectral amplitudes $x^{ms}(\psi)$ and $x^{mc}(\psi)$ appear in the series for both $x(\psi, \theta)$ and $z(\psi, \theta)$. This has been shown by Weitzner [5] to be a complete representation for a two-dimensional closed curve.

Note that up–down symmetry has not been assumed, i.e., neither $x(\psi, \theta)$ nor $z(\psi, \theta)$ has specific parity about the origin $\theta = 0$. The presence of both the sine and cosine terms in the series for x and z is necessary to represent a general up–down asymmetric two-dimensional closed curve. When up–down symmetry is present, only a cosine series for x and a sine series for z suffice, i.e., $x^{ms} = z^{1c} = z^{0c} = 0$. The term proportional to $\sin\theta$ in Eq. (13a) can always be made to vanish by an appropriate choice of the origin for the angle θ.

With the spectral representation of x and z given by Eq. (13), the Lagrangian density L is a function of all the spectral amplitudes and their ψ-derivatives. The variational principle gives a natural way of arriving at the differential equations for the spectral amplitudes. Varying the action integral A with respect to the poloidal flux and the spectral amplitudes, we obtain the following Euler–Lagrange equations:

$$\left\langle \frac{\partial L}{\partial \chi} - \frac{d}{d\psi} \frac{\partial L}{\partial \chi_\psi} \right\rangle = 0, \tag{14}$$

$$\left\langle \frac{\partial L}{\partial E} - \frac{d}{d\psi} \frac{\partial L}{\partial E_\psi} \right\rangle = 0, \tag{15a}$$

$$\left\langle \frac{\partial L}{\partial x^{mc}} - \frac{d}{d\psi} \frac{\partial L}{\partial x^{mc}_\psi} \right\rangle = 0, \qquad m = 0, 2, 3, \ldots, M, \tag{15b}$$

$$\left\langle \frac{\partial L}{\partial z^{mc}} - \frac{d}{d\psi} \frac{\partial L}{\partial z^{mc}_\psi} \right\rangle = 0, \qquad m = 0, 1, \tag{15c}$$

$$\left\langle \frac{\partial L}{\partial x^{ms}} - \frac{d}{d\psi}\frac{\partial L}{\partial x^{ms}_{\psi}} \right\rangle = 0, \qquad m = 2, 3, \ldots, M, \tag{15d}$$

where the subscript ψ denotes derivative with respect to ψ, and $\langle\ \rangle$ is the poloidal angle averaging operator defined by

$$\langle A \rangle = \frac{1}{2\pi}\int_0^{2\pi} A\, d\theta \tag{16a}$$

for some function A. Its relation to the volume-weighted flux surface averaging operator $\langle A \rangle_f$ is

$$\langle A \rangle_f = \langle JA \rangle / \langle J \rangle. \tag{16b}$$

It is also useful to define the differential volume V_ψ as

$$V_\psi \equiv \frac{dV}{d\psi} = 2\pi \int_0^{2\pi} J\, d\theta. \tag{17}$$

We note here that Eqs. (14) and (15) can be written in terms of the operator G defined in Eq. (11),

$$\langle JG \rangle = 0, \tag{18}$$

$$\langle (xz_\theta \cos\theta + E^{-2} x x_\theta \sin\theta)\, G \rangle = 0, \tag{19a}$$

$$\langle (-xz_\theta \cos m\theta + \sigma_{s,m} x x_\theta \sin m\theta)\, G \rangle = 0, \qquad m = 0, 2, 3, \ldots, M, \tag{19b}$$

$$\langle (x x_\theta \cos m\theta)\, G \rangle = 0, \qquad m = 0, 1, \tag{19c}$$

$$\langle (-xz_\theta \sin m\theta + \sigma_{a,m} x x_\theta \cos m\theta)\, G \rangle = 0, \qquad m = 2, 3, \ldots, M. \tag{19d}$$

From the form of Eq. (19), we see that the variational method summarized by Eq. (15) is equivalent to multiplying the flux coordinate form of the equilibrium equation $G = 0$, Eq. (11), by appropriate combinations of $\sin m\theta$ and $\cos m\theta$, and then averaging over the θ dependence. The variational method gives an optimal prescription for taking the angular moments once a truncated set of basis functions is chosen.

It is convenient to introduce some new notation. Let

$$\vec{S} \equiv (E, x^{0c}, x^{2c}, x^{3c}, z^{0c}, z^{1c}, x^{2s}, x^{3s})^{\mathrm{T}} \tag{20a}$$

be the spectral vector for the first three harmonics and

$$\vec{s} \equiv (x^{4c}, x^{5c}, \ldots, x^{Mc}, x^{4s}, x^{5s}, \ldots, x^{Ms})^{\mathrm{T}} \tag{20b}$$

be that for the higher harmonics. Here the superscript T denotes the transpose of a vector. Then Eq. (19) can be written in the form

$$\vec{A}(\vec{S}, \vec{S}_\psi, \vec{s}, \vec{s}_\psi, \psi) \cdot \vec{S}_{\psi\psi} + \vec{D}(\vec{S}, \vec{S}_\psi, \vec{s}, \vec{s}_\psi, \vec{s}_{\psi\psi}, \psi) = 0, \tag{21}$$

$$\vec{a}(\vec{S}, \vec{S}_\psi, \vec{s}, \vec{s}_\psi, \psi) \cdot \vec{s}_{\psi\psi} + \vec{d}(\vec{S}, \vec{S}_\psi, \vec{S}_{\psi\psi}, \vec{s}, \vec{s}_\psi, \psi) = 0. \tag{22}$$

Here $\vec{A}$ is an 8×8 matrix, $\vec{D}$ an 8×1 matrix, $\vec{a}$ a $2(M-3) \times 2(M-3)$ matrix, and $\vec{d}$ a $2(M-3) \times 1$ matrix. The elements of $\vec{A}$, $\vec{D}$, $\vec{a}$, and $\vec{d}$ are given in Appendix B. In Eqs. (21) and (22) we have suppressed the dependence on χ, χ_ψ, and $\chi_{\psi\psi}$.

Equation (18) can be interpreted as a defining equation for the poloidal flux χ once the geometry, the pressure $p(\chi)$, and the toroidal field function $g(\chi)$ are given. It can be explicitly written as

$$\chi_{\psi\psi} \left\langle \frac{x_\theta^2 + z_\theta^2}{J} \right\rangle + \chi_\psi \left[\left\langle \frac{x_\theta^2 + z_\theta^2}{J} \right\rangle \right]_\psi + \langle J \rangle \frac{dp}{d\chi} + R_0^2 \left\langle \frac{J}{x^2} \right\rangle g \frac{dg}{d\chi} = 0 \tag{23a}$$

or

$$\chi_{\psi\psi} \left\langle \frac{x_\theta^2 + z_\theta^2}{J^2} \right\rangle_f V_\psi + \chi_\psi \left[V_\psi \left\langle \frac{x_\theta^2 + z_\theta^2}{J^2} \right\rangle_f \right]_\psi + V_\psi \frac{dp}{d\chi} + R_0^2 V_\psi \langle x^{-2} \rangle_f g \frac{dg}{d\chi} = 0. \tag{23b}$$

Alternatively, instead of $p(\chi)$ and $g(\chi)$, we may prescribe $p(\chi)$ and the safety factor $q(\chi)$, where $q(\chi)$ and $g(\chi)$ are related through

$$R_0^2 g \frac{dg}{d\chi} \langle J/x^2 \rangle = q \left[\frac{q\chi_\psi}{\langle J/x^2 \rangle} \right]_\psi, \tag{24a}$$

or

$$R_0^2 g \frac{dg}{d\chi} \langle x^{-2} \rangle_f V_\psi = q \left[\frac{(2\pi)^4 q\chi_\psi}{\langle x^{-2} \rangle_f V_\psi} \right]_\psi. \tag{24b}$$

Substitution of Eq. (24) into Eq. (23) yields the alternative form

$$\chi_{\psi\psi} \left[\frac{q^2}{\langle J/x^2 \rangle} + \left\langle \frac{x_\theta^2 + z_\theta^2}{J} \right\rangle \right] + \chi_\psi \left\{ q \left[\frac{q}{\langle J/x^2 \rangle} \right]_\psi + \left[\left\langle \frac{x_\theta^2 + z_\theta^2}{J} \right\rangle \right]_\psi \right\} + \langle J \rangle \frac{dp}{d\chi} = 0, \tag{25a}$$

or

$$\chi_{\psi\psi} \left\{ \frac{(2\pi)^4 q^2}{V_\psi \langle x^{-2} \rangle_f} + V_\psi \left\langle \frac{x_\theta^2 + z_\theta^2}{J^2} \right\rangle_f \right\} + \chi_\psi \left\{ (2\pi)^4 q \left[\frac{q}{\langle x^{-2} \rangle_f V_\psi} \right]_\psi + \left[V_\psi \left\langle \frac{x^2 + z_\theta^2}{J^2} \right\rangle_f \right]_\psi \right\} + V_\psi \frac{dp}{d\chi} = 0. \tag{25b}$$

The functions $p(\chi)$ and $g(\chi)$, or $p(\chi)$ and $q(\chi)$, are normally given as simple power law functions of the normalized poloidal flux $\chi/\Delta\chi$ where $\Delta\chi \equiv \chi_l - \chi_0$, with $\chi_l \equiv \chi$ $(\psi = 1)$ and $\chi_0 \equiv \chi$ $(\psi = 0)$. Typically, we take the functional forms as follows:

$$p(\chi) = p_{\min} + (p_0 - p_{\min})[(\chi_l - \chi)/\Delta\chi]^{\alpha_1},$$
$$g(\chi) = 1 - [g_p(\chi_l - \chi)/\Delta\chi]^{\alpha_2},$$
$$q(\chi) = q_0\{2/[1 + 3(\chi - \chi_l)/\Delta\chi]^{1/2}\}^{\alpha_3}.$$

Here p_0 and $p_{\min}$ are the peak and minimum pressures, g_p is a constant, and q_0 is the safety factor on-axis.

The nature of Eqs. (18) and (19) becomes more transparent through Eqs. (21), (22), and (23) or (25), which form a system of second-order, nonlinear, coupled ordinary differential equations (ODE's) to be solved for the poloidal flux χ, the ellipticity E, and the mode amplitudes x^{mc}, x^{ms}, z^{0c}, z^{1c}, as a boundary value problem.

C. *Boundary Conditions*

Two boundary conditions, one at $\psi = 0$ (magnetic axis) and one at $\psi = 1$ (boundary), are needed to solve each of the coupled second-order ODE's. However, the center point $\psi = 0$ is not a physical boundary but rather a singularity in the coordinate system. Thus we are only free to specify the boundary spectral amplitudes E_b, x_b^{0c}, z_b^{0c}, z_b^{1c}, x_b^{mc}, and x_b^{ms} for $m \geq 2$, the subscript b denoting boundary values. The boundary conditions at $\psi = 0$ are essential boundary conditions.

To obtain these essential boundary conditions, χ is assumed to be analytic at the magnetic axis and to have an extremum at $\psi = 0$. It follows that the spectral amplitudes and χ have the following asymptotic behavior as ψ approaches 0:

$$\begin{aligned}
E &\sim E_0 + E_1\psi + \cdots, \\
x^{0c} &\sim x_0 + x_1^{0c}\psi + \cdots, \\
z^{0c} &\sim z_0 + z_1^{0c}\psi + \cdots, \\
z^{1c} &\sim z_0^{1c} + z_1^{1c}\psi + \cdots, \\
x^{mc} &\sim x_1^{mc}\psi + \cdots, \qquad m \geq 2, \\
x^{ms} &\sim x_1^{ms}\psi + \cdots, \qquad m \geq 2, \\
\chi &\sim \chi_0 + \chi_1\psi + \chi_2\psi^2 + \cdots.
\end{aligned} \tag{26}$$

Thus, the amplitudes $x^{mc}\psi^{(m-2)/2}$ and $x^{ms}\psi^{(m-2)/2}$ for $m \geq 2$ in Eq. (13) go to zero like $\psi^{m/2}$ as $\psi \to 0$. Numerically, we find it useful to factor out the $\psi^{(m-2)/2}$ explicitly so that x^{mc} and x^{ms} are proportional to ψ as ψ approaches 0, and x_ψ^{mc}, x_ψ^{ms} do not vanish at $\psi = 0$. Substituting Eq. (26) into Eqs. (21), (22), and (23), we obtain

derivative boundary conditions at $\psi = 0$. For up–down symmetric elliptical flux surfaces, we have

$$x_1^{0c} = \frac{-T}{2x_0(E_0^2 + 3E_0^{-2})}\left(1 - \frac{p'(0)\, E_0^2 x_0^2 T}{\chi_1}\right), \tag{27a}$$

$$E_1 = \frac{1}{(1+E_0^{-4})}\left\{\frac{T}{6E_0 x_0^2} - \frac{E_0 T^2 p'(0)}{24\chi_1} + \frac{2(x_1^{0c})^2}{TE_0^5} + \frac{x_1^{0c}}{6E_0 x_0}(E_0^2 + 4E_0^{-2}) - \frac{\chi_2}{3\chi_1}(E_0 - E_0^{-3})\right\}, \tag{27b}$$

$$\chi_1 = -\frac{T}{2(E_0^2 + E_0^{-2})}(R_0^2(gg')_0 + p'(0)\, x_0^2). \tag{27c}$$

Here,

$$p'(0) \equiv \left(\frac{dp}{d\chi}\right)_{\chi=\chi_0}, \qquad (gg')_0 \equiv \left(g\frac{dg}{d\chi}\right)_{\chi=\chi_0}. \tag{28}$$

Furthermore, if the flux surfaces are circular ($E_0 = 1$), Eq. (27) reduces to

$$x_1^{0c} = -\frac{T}{8x_0}\left(1 - \frac{Tp'(0)\, x_0^2}{\chi_1}\right), \tag{29a}$$

$$\chi_1 = -\frac{T}{4}(R_0^2(gg')_0 + x_0^2 p'(0)). \tag{29b}$$

Equations (29a,b) are seen to agree with standard results [6].

For the more general case with up–down asymmetry and higher harmonics, we have used MACSYMA to obtain the derivative boundary conditions and found that only terms up to and including the third harmonic appear. These conditions have the following functional forms:

$$E_1 = f_1(x_0, E_0, z_0^{1c}, x_1^{0c}, z_1^{0c}, z_1^{1c}, x_1^{2c}, x_1^{2s}, x_1^{3c}, x_1^{3s}), \tag{30a}$$

$$x_1^{0c} = f_2(x_0, E_0, z_0^{1c}, z_1^{0c}, x_1^{2c}, x_1^{2s}), \tag{30b}$$

$$z_1^{0c} = f_3(x_0, E_0, z_0^{1c}, x_1^{0c}, x_1^{2c}, x_1^{2s}), \tag{30c}$$

$$z_1^{1c} = f_4(x_0, E_0, z_0^{1c}, x_1^{0c}, z_1^{0c}, E_1, x_1^{2c}, x_1^{2s}, x_1^{3c}, x_1^{3s}). \tag{30d}$$

For the up–down symmetric case, only E_1 and x_1^{0c} are nonvanishing and they are given in Appendix A. Note that all the derivatives are coupled in a very nonlinear fashion at the magnetic axis.

In summary, for the fixed-boundary problem, the boundary conditions on the geometrical harmonics are: (a) At $\psi = 1$, prescribe the boundary amplitudes $\vec{S}_b$, $\vec{s}_b$,

and $\chi_1 \equiv \chi(1)$. (b) At $\psi = 0$, the derivative boundary conditions on the zeroth and first harmonics are given by Eqs. (30) which can be put in the form

$$\vec{B} \cdot \Delta\psi \vec{S}_\psi |_{\psi=0} = \vec{R}. \tag{31}$$

For $m \geqslant 2$, $x^{mc} = 0$ and $x^{ms} = 0$ at $\psi = 0$.

The boundary condition at the origin for the poloidal flux depends on which form is being used, Eq. (23) or Eq. (25). When using Eq. (23) in which $p(\chi)$ and $g(\chi)$ are given functions, the equation does not allow a boundary value to be imposed at the origin, but rather we find from expanding that the derivative condition

$$\chi_1 = \frac{-T[x_0^2 p'(0) + R_0^2 (gg')_0]}{2[E_0^2 + E_0^{-2} + (z_0^{1c})^2/T]} \tag{32}$$

must be imposed. In contrast, when using Eq. (25) in which $p(\chi)$ and $q(\chi)$ are prescribed functions, the boundary value for χ at the origin, χ_0, must be given.

D. *Free Boundary Formulation*

In Section C we described how to obtain a self-consistent plasma equilibrium solution when the shape of the plasma–vacuum interface is known. Here we discuss how to obtain that boundary shape self-consistently once a set of discrete coil currents are prescribed.

The magnetic field in the vacuum is represented as

$$\vec{B}_{\text{vac}} = \nabla\phi \times \nabla\chi + R_0 g_0 \nabla\phi, \tag{33}$$

where the overall constant B_0 has been suppressed. The vacuum poloidal flux per radian satisfies

$$\Delta^* \chi = \sum_{n=1}^{N} I_n \delta(\vec{x} - \vec{x}_n).$$

Here $\vec{x}_r \equiv (x_r, z_r)$ and $(I_n, \vec{x}_n; n = 1, N)$ are the currents and locations of external coils. An application of Green's theorem yields

$$\chi(\vec{x}_r) = \frac{1}{2\pi} \sum_{n=1}^{N} I_n G(\vec{x}_r, \vec{x}_n) + \frac{1}{2\pi} \oint \frac{dl_s}{x_s} G(\vec{x}_r, \vec{x}_s) \frac{\partial\chi(\vec{x}_s)}{\partial n_s}, \tag{34}$$

the integral being over the plasma–vacuum interface, $\psi = 1$. Here $G(\vec{x}_r, \vec{x}_s)$ is the infinite medium Green's function given by

$$G(\vec{x}_r, \vec{x}_s) = -(x_r x_s)^{1/2} k^{-1} ((2 - k^2) K(k) - 2E(k)) \tag{35}$$

with $K(k)$ and $E(k)$ being complete elliptic integrals of the first and second kind with

$$k^2 \equiv \frac{4x_r x_s}{[(x_r + x_s)^2 + (z_r - z_s)^2]}. \tag{36}$$

At the plasma–vacuum boundary, the coordinates x_b and z_b have the spectral representation given by Eq. (13) with $\psi = 1$. Then Eq. (34) gives, for $\vec{x}_r = \vec{x}_b(\theta)$,

$$\chi(\vec{x}_b(\theta)) = \chi_b' \left\langle \left(\frac{x_{\theta'}^2 + z_{\theta'}^2}{J(\theta')} \right)_b G(\vec{x}_b(\theta'), \vec{x}_b(\theta)) \right\rangle_{\theta'} + \frac{1}{2\pi} \sum_{n=1}^{N} I_n G(\vec{x}_b(\theta), \vec{x}_n), \tag{37}$$

where $\langle\ \rangle_{\theta'}$ denotes poloidal angle average over θ'. In Eq. (37) the integral over θ' has an integrable singularity when $\theta' = \theta$. When the integral becomes a finite sum, this becomes the "self-field" (SF) contribution [7] that we now evaluate. From Eq. (34), we see that the self-field contribution is given by

$$\mathrm{SF} = \frac{1}{2\pi} \left[\frac{\partial \chi}{\partial n} \right]_{\vec{x}_r} \frac{1}{x_r} \int_{-\Delta l_s/2}^{+\Delta l_s/2} dl_s\, G(\vec{x}_r, \vec{x}_s),$$

where $\vec{x}_s$ is close to $\vec{x}_r$ so that we have

$$x_s = x_r + x_{\theta'}\, \Delta\theta' + \tfrac{1}{2} x_{\theta'\theta'} (\Delta\theta')^2 + \cdots,$$
$$z_s = z_r + z_{\theta'}\, \Delta\theta' + \tfrac{1}{2} z_{\theta'\theta'} (\Delta\theta')^2 + \cdots,$$

with $\Delta l_s \equiv \Delta\theta' (x_{\theta'}^2 + z_{\theta'}^2)^{1/2}$. Then $k^2 \simeq 1 - \delta^2$ where $\delta \equiv \Delta l_s / 2x_r$, and $G(\vec{x}_r, \vec{x}_s) \simeq x_r [\ln \delta - 2(\ln 2 - 1)]$. Finally, the self-field contribution is given by

$$\mathrm{SF} = \frac{1}{2\pi} \left[\frac{\partial \chi}{\partial n} \right]_{\vec{x}_r} \Delta l_s \left[\ln \left(\frac{\Delta l_s}{16 x_r} \right) + 1 \right].$$

Since the plasma–vacuum boundary is a flux surface, χ on the boundary should be equal to a constant, χ_b. Ideally, $\chi(\vec{x}_b(\theta))$ should equal χ_b, but since we have a finite representation for x_b and z_b, $\chi(\vec{x}_b(\theta))$ differs from χ_b by some error. A measure of this is the mean-square error

$$\varepsilon \equiv \frac{1}{2\pi} \int_0^{2\pi} d\theta\, W(\theta) [\chi_b - \chi(\vec{x}_b(\theta))]^2, \tag{38}$$

where $W(\theta)$ is some positive definite weighting function which is usually set to 1. Note that ε is a function of χ_b, $\vec{S}_b$, and $\vec{s}_b$.

We minimize ε with respect to χ_b, $\vec{S}_b$, and $\vec{s}_b$. Setting $(\partial\varepsilon/\partial\chi_b)=0$ gives

$$\chi_b = \langle \chi(\vec{x}_b(\theta)) \rangle \tag{39}$$

while $\partial\varepsilon/\partial\vec{S}_b = 0$ and $\partial\varepsilon/\partial\vec{s}_b = 0$ give

$$\partial\varepsilon/\partial\vec{S}_b \equiv \vec{P}(\vec{S}_b, \vec{s}_b) = 0 \tag{40a}$$

and

$$\partial\varepsilon/\partial\vec{s}_b \equiv \vec{p}(\vec{S}_b, \vec{s}_b) = 0. \tag{40b}$$

Equations (40) form a system of nonlinear coupled algebraic equations in the boundary spectral amplitudes $\vec{S}_b$ and $\vec{s}_b$. A free-boundary equilibrium consistent with currents in external coils and conductors is obtained by solving Eqs. (40), (21), (22), and (23) or (25) self-consistently.

III. Method of Solution

A. *Fixed-Boundary Solution: Quasilinearization and Finite-Difference*

Since the second-order ordinary differential equations derived here are nonlinear, an iteration procedure is needed to solve them. We employ quasilinearization which is an application of the Newton–Raphson–Kantorovich approximation method in function space. The resulting sequence of ODE's is then solved by using the finite-difference method.

To solve the fixed-boundary problem, we first solve the poloidal flux equation [Eq. (23) or Eq. (25)] for χ by iteration while holding the geometry $[\vec{S}(\psi), \vec{s}(\psi)]$ fixed. Next we advance the geometry one step while holding χ fixed. Then we go back and solve the poloidal flux equation again and repeat the whole procedure until $\vec{S}(\psi)$ and $\vec{s}(\psi)$ have converged. This iterative procedure is described by the inner loop with cycle index k in the flow chart shown in Fig. 2. The relaxation parameters ν, θ_i, ω_m for $i = 1,..., 8$ and $m = 1,..., 2(M-3)$ take on values between 0 and 1. The solution of the nonlinear ODE's for χ, $\vec{S}$, and $\vec{s}$ is discussed in more detail below.

The differential equation for χ, Eq. (23) or Eq. (25), can be written as

$$\chi_{\psi\psi} = f(\chi, \chi_\psi, \psi), \tag{41}$$

where the dependence on geometry $[\vec{S}(\psi), \vec{s}(\psi)]$ has been suppressed in the function f. Quasilinearization [8] yields the following sequence of differential equations:

$$\begin{aligned} \chi^{n+1}_{\psi\psi} = {} & f(\chi^n, \chi^n_\psi, \psi) + f_\chi(\chi^n, \chi^n_\psi, \psi)(\chi^{n+1} - \chi^n) \\ & + f\chi_\psi(\chi^n, \chi^n_\psi, \psi)(\chi^{n+1}_\psi - \chi^n_\psi), \\ n = {} & 0, 1, 2,\ldots . \end{aligned} \tag{42}$$

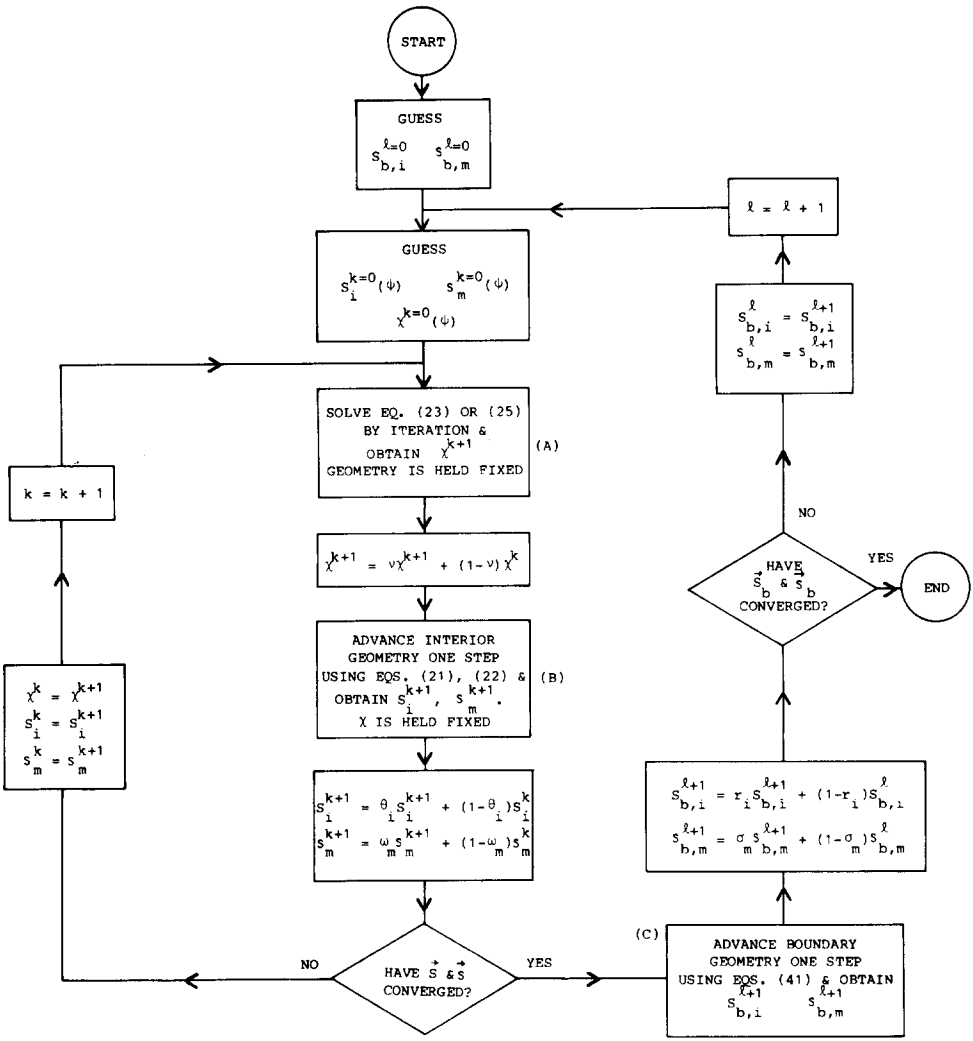

FIG. 2. Flow chart showing the nest of iterations. The components of $(\vec{S}, \vec{S}_b)$ and $(\vec{s}, \vec{s}_b)$ are indicated by the subscript i and m, respectively, for $i = 1,..., 8$ and $m = 1,..., 2(M-3)$. The relaxation parameters ν, θ_i, ω_m, Ω_i, and σ_m take on values between 0 and 1.

After central differencing in ψ, Eq. (42) gives a finite-difference equation of the form

$$a_j \chi_{j+1}^{n+1} - b_j \chi_j^{n+1} + c_j \chi_{j-1}^{n+1} + d_j = 0, \tag{43}$$

for $j = 1,..., N_\psi$ where N_ψ is the number of grid points in ψ. We assume a recursive solution of the form

$$\chi_j^{n+1} = e_j \chi_{j+1}^{n+1} + f_j. \tag{44}$$

This implies that e_j and f_j obey the recursive relations

$$e_j = \frac{a_j}{b_j - c_j e_{j-1}} \tag{45}$$

and

$$f_j = \frac{d_j + c_j f_{j-1}}{b_j - c_j e_{j-1}}. \tag{46}$$

Equation (44) is solved by first specifying e_1 and f_1 and solving Eqs. (45) and (46) recursively for $e_j, f_j; j = 2, N_\psi - 1$. These coefficients are then used in evaluating the backward recursive solution, Eq. (44), once $\chi_{N_\psi}^{n+1}$ is given. The value of χ at the boundary is χ_l so that $\chi_{N_\psi}^{n+1} = \chi_l$. Without loss of generality, we take χ_l to be zero. The values of e_1 and f_1 are determined by the boundary condition at the magnetic axis. For the q-solver form, Eq. (25), we specify $\chi_0 \equiv \chi$ $(\psi = 0)$; thus $e_1 = 0$, and $f_1 = \chi_0$. For the g-solver form, Eq. (23), we have a derivative boundary condition on χ given by Eq. (32). Then $e_1 = 1$ and $f_1 = -\Delta\psi\, \chi_\psi$ $(\psi = 0) - 1/2(\Delta\psi)^2\, \chi_{\psi\psi}$ $(\psi = 0)$. Here $\Delta\psi$ is the grid size and is given by

$$\Delta\psi = \frac{1}{N_\psi - 1}. \tag{47}$$

Equation (43) is solved iteratively until χ has converged for some $n = N_\chi$ with the geometry held fixed (Box A in Fig. 2).

Quasilinearization of the differential equations for the spectral amplitudes, Eqs. (21) and (22), gives

$$(\vec{A} \cdot \vec{S}_{\psi\psi}^{k+1})_i + \left(\frac{\partial D_i}{\partial S_i}\right)^k (S_i^{k+1} - S_i^k) + \left(\frac{\partial D_i}{\partial S_{\psi,i}}\right)^k (S_{\psi,i}^{k+1} - S_{\psi,i}^k) + D_i^k = 0 \tag{48}$$

for $i = 1,..., 8$ and

$$a_{mm} s_{\psi\psi,m}^{k+1} + \left(\frac{\partial d_m}{\partial s_m}\right)^k (s_m^{k+1} - s_m^k) + \left(\frac{\partial d_m}{\partial s_{\psi,m}}\right)^k (s_{\psi,m}^{k+1} - s_{\psi,m}^k) + d_m^k = 0 \tag{49}$$

for $m = 1,..., 2(M-3)$. Here we want to solve for the spectral amplitudes at the $(k+1)$th fixed-boundary iteration step, $\vec{S}^{k+1}$ and s^{k+1}, given that we already know $\vec{S}^k$ and s^k. Finite-differencing Eq. (48), we obtain an equation of the form

$$\vec{A}_j^k \cdot \vec{S}_{j+1}^{k+1} - \vec{B}_j^k \cdot \vec{S}_j^{k+1} + \vec{C}_j^k \cdot \vec{S}_{j-1}^{k+1} + \vec{D}_j^k = 0. \tag{50}$$

Equation (50) is the matrix version of Eq. (43) and is solved in an analogous way. Let

$$\vec{S}_j^{k+1} = \vec{E}_j^k \cdot \vec{S}_{j+1}^{k+1} + \vec{F}_j^k. \tag{51}$$

Then we have the recursive relations

$$\vec{\vec{E}}_j^k = (\vec{\vec{B}}_j^k - \vec{\vec{C}}_j^k \cdot \vec{\vec{E}}_{j-1}^k)^{-1} \cdot \vec{\vec{A}}_j^k \tag{52a}$$

and

$$\vec{\vec{F}}_j^k = (\vec{\vec{B}}_j^k - \vec{\vec{C}}_j^k \cdot \vec{\vec{E}}_{j-1}^k)^{-1} \cdot (\vec{\vec{D}}_j^k + \vec{\vec{C}}_j^k \cdot \vec{\vec{F}}_{j-1}^k). \tag{52b}$$

At the boundary we specify $\vec{S}_b^l$ where l is the free-boundary iteration step; thus $\vec{S}_{N_\psi}^{k+1} = \vec{S}_b^l$. At the magnetic axis, $\vec{\vec{F}}_1^k$ and $\vec{\vec{E}}_1^k$ are obtained from Eq. (31). We solve Eq. (49) in exactly the same way except that here $\vec{\vec{E}}_1^k = 0$ and $\vec{\vec{F}}_1^k = 0$. Thus we have advanced $\vec{S}^k$ and $\vec{s}^k$ to $\vec{S}^{k+1}$ and $\vec{s}^{k+1}$ (Box B in Fig. 2).

B. *Free-Boundary Solution: Newton's Iteration*

The nonlinear algebraic system of equations for the boundary spectral amplitudes, Eqs. (40), are solved by the Newton–Raphson method:

$$\vec{S}_b^{l+1} = \vec{S}_b^l - \vec{\vec{J}}^{-1} \cdot \vec{P}(\vec{S}_b^l, \vec{s}_b^l), \tag{53a}$$

$$\vec{s}_{b,m}^{l+1} = \vec{s}_{b,m}^l - \vec{\vec{j}}^{-1} \cdot \vec{p}_m(\vec{S}_b^l, \vec{s}_b^l), \qquad m = 1,..., 2(M-3). \tag{53b}$$

Here,

$$J_{ij} \equiv \left(\frac{\partial P_i}{\partial S_{b,j}}\right)^l = \left(\frac{\partial^2 \varepsilon}{\partial S_{b,i}\, \partial S_{b,j}}\right)^l$$

and

$$j_{mn} \equiv \left(\frac{\partial p_m}{\partial s_{b,n}}\right)^l = \left(\frac{\partial^2 \varepsilon}{\partial s_{b,m}\, \partial s_{b,n}}\right)^l.$$

For the higher harmonics ($m > 3$), we assume a diagonal $\vec{j}$ matrix. Note that $\vec{\vec{J}}$ is essentially the Hessian [9] of the mean-square error ε (for $m = 3$), and a sufficient condition for a solution of Eq. (53a) to give a minimum ε is that $\vec{\vec{J}}$ be positive-definite. Indeed for all the free-boundary equilibria shown in Section V, $\vec{\vec{J}}$ is positive-definite and ε is a minimum. Equations (53) show the manner in which $\vec{S}_b$ and $\vec{s}_b$ are advanced in the free-boundary iteration (Box C in Fig. 2). The whole nest of iterations is depicted in the flow chart in Fig. 2.

IV. Code Verification

A. *Fixed Boundary*

The accuracy of the numerical solution to the equilibrium equation is measured by a root-mean-square (rms) error which is obtained by substituting the final solution into the inverse Grad–Shafranov equation, Eq. (11), and calculating an average residual error. In Fig. 3, the logarithm of the rms error is plotted versus the

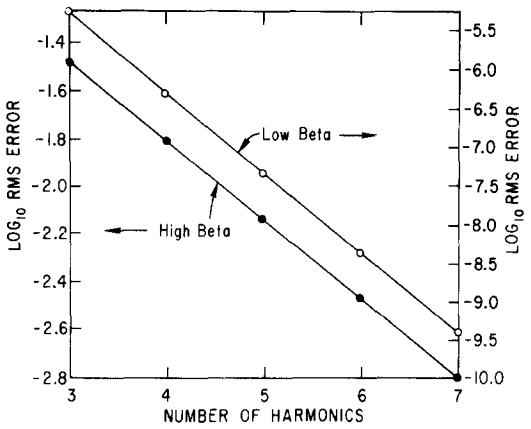

FIG. 3. The logarithm of the rms error versus the number of harmonics for both high-β (19.6%) and low-β (0.26%) equilibrium.

TABLE I

Parameter Values for the Low-β and High-β Fixed-Boundary Equilibria in Fig. 3, the $\beta = 2.5\%$ Equilibrium Considered in Figs. 4 to 7, and the Free-Boundary TFTR Equilibrium of Table II

Parameters	Low β	High β[b]	Figs. 4–7	TFTR
χ_0[a]	−0.083	−0.076	−0.3457	−0.083
p_0	0.004	0.25	0.0373	0.004
$p_{\min}$	0.0	0.0	0.00001	0.0
α_1	2.0	2.0	2.0	2.0
q_0	1.0	1.0	1.1	1.0
α_3	1.325	1.325	1.0	1.325
B_0 (kg)	15.0	15.0	10.0	15.0
R_0 (m)	2.50	2.50	4.0	2.50
$\sqrt{T}$ (m)	0.50	0.50	1.0	0.50
x_b^{0c} (m)	2.576	2.576	4.0	—
E_b	1.0	1.0	1.0	—
x_b^{2c} (m)	0	0	0	—
x_b^{3c} (m)	0	0	0	—
x_b^{4c} (m)	0	0	0	—
x_b^{5c} (m)	0	0	0	—
x_b^{6c} (m)	0	0	0	—
x_b^{7c} (m)	0	0	—	—
N_ψ	21	21	11–81	11
$\langle\beta\rangle$	0.26%	19.6%	2.5%	0.26%

[a] χ_0 is the initial value of the poloidal flux at the magnetic axis. It is adjusted every iteration step such that the toroidal field function g is 1 at the edge.

[b] Figure 14 gives the equilibrium plots for this case.

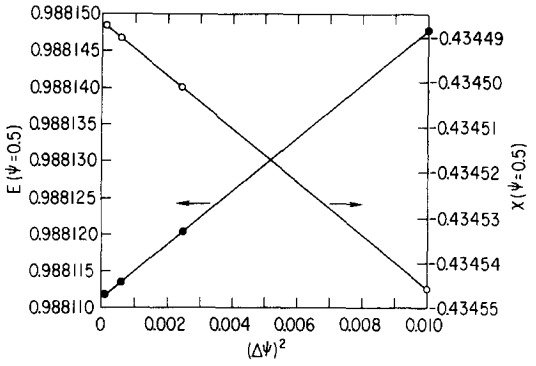

FIG. 4. The poloidal flux χ and the ellipticity E at flux surface $\psi = 0.5$ versus the square of the grid size $(\Delta\psi)^2$.

number of harmonics, and for both a low-β (0.26%) and a high-β (19.6%) up–down symmetric fixed-boundary solution. A negatively sloped straight line plot is obtained, indicating the exponential decay of the rms error, characteristic of a spectral method. The rms error for the high-β case is several orders of magnitude larger than that for the low-β case, indicating that many more harmonics are needed to achieve the same accuracy. For both cases, the outermost flux surface is [illegible] and details of the various parameter values are given in Table I. The unit [illegible] follows. The pressure p (e.g., p_0 or $p_{\min}$) is measured in units of μ_0/B_0^2 where $\mu_0 = 4\pi \times 10^{-7}$ henry/meter is the vacuum magnetic permeability, i.e., the real pressure in MKS units is $p_{\text{real}} = pB_0^2/\mu_0$ newtons/meter^2 with B_0 given in teslas. The poloidal flux χ (e.g., χ_0) has the dimension of meter^2 and the real poloidal flux $\chi_{\text{real}} = 2\pi B_0 \chi$ webers.

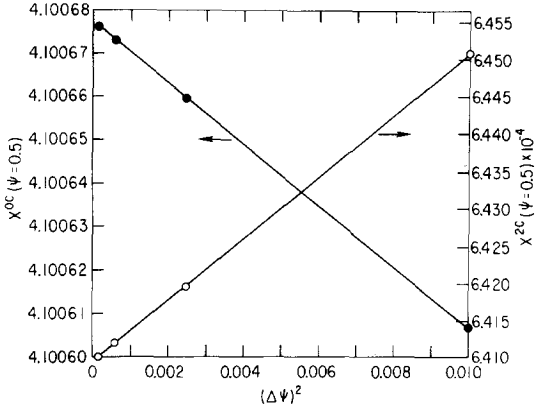

FIG. 5. The zeroth harmonic x^{0c} and the second harmonic x^{2c} at $\psi = 0.5$ versus the square of the grid size $(\Delta\psi)^2$.

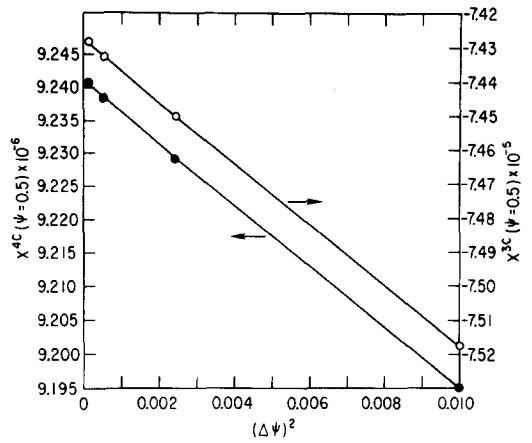

FIG. 6. The third harmonic x^{3c} and the fourth harmonic x^{4c} at $\psi = 0.5$ versus the square of the grid size $(\Delta\psi)^2$.

To check the accuracy of the finite-difference scheme, various quantities are plotted versus the grid-size squared $(\Delta\psi)^2$ in Figs. 4 to 7. In Fig. 4 the ellipticity E and poloidal flux χ at the flux surface with flux label $\psi = 0.5$ are plotted. Straight line plots show that the convergence is of second order as is expected since a second-order central differencing scheme has been used. Similar results are shown in Fig. 5, where the zeroth and second-harmonic amplitude at $\psi = 0.5$ are plotted. In Figs. 6 and 7, higher harmonic amplitudes at $\psi = 0.5$ are plotted. The point corresponding to ten flux surfaces, or $\Delta\psi = 0.1$, is seen to deviate from the straight line plot. As the

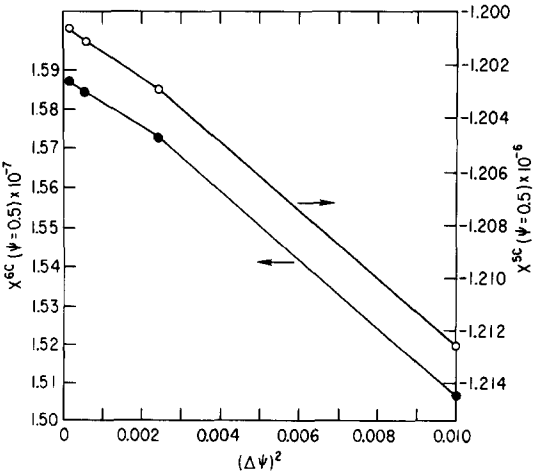

FIG. 7. The fifth harmonic x^{5c} and the sixth harmonic x^{6c} at $\psi = 0.5$ versus the square of the grid size $(\Delta\psi)^2$.

TABLE II

The Mean-Square Error ε as a Function of the Number of Spectral Harmonics N_H

N_H	ε
3	2.2×10^{-11}
4	3.8×10^{-12}
5	1.7×10^{-13}
6	7.8×10^{-14}

TABLE III

External Conducting Coils for TFTR

Line currents (A)	x (m)	z (m)	n_T (number of turns)
Ohmic-heating coils:			
$I_{OH} = 8000$	0.659	0.253	100
	0.767	1.003	71
	0.928	0.971	4
	0.943	1.066	11
	1.002	1.098	2
	1.198	1.573	26
	1.604	1.842	18
	2.332	2.138	9
	3.878	2.085	6
	4.982	0.673	2
Equilibrium-field coils:			
$I_{EF} = 3000$	0.670	0.758	40
	0.793	0.792	7
	0.834	0.826	2
	2.839	2.146	−9
	3.880	1.949	−14
	4.874	0.781	−26
Variable-curvature coils:			
$I_{VC} = -3000$	0.717	1.465	−27
	1.604	2.020	15
	2.332	2.290	4
	4.982	0.851	−3

number of harmonics is increased, the grid size has to be refined to ensure second-order convergence in $\Delta\psi$ for these higher harmonics. The particular up–down symmetric fixed boundary equilibrium considered in Figs. 4 to 7 has a circular outermost flux surface with the remaining parameters also given in Table I.

B. *Free Boundary*

In the free-boundary iteration, insight into the convergence properties is gained by plotting the mean-square error ε and the boundary spectral amplitudes versus the iteration step. A plot for a case discussed below is shown in Fig. 9e, where $\log \varepsilon$ and the third-harmonic boundary amplitude x_b^{3c} are plotted. The convergence is quite dramatic.

Another important verification of the code is the behavior of the mean-square error ε as the number of harmonics N_H is increased. The converged value of ε is expected to decrease as N_H increases since now there is more freedom in fine tuning the boundary shape such that the poloidal flux is as close to a constant as possible. Table II shows that indeed ε decreases as the number of harmonics increases for a TFTR equilibrium whose parameters and external conducting coils are listed in Table I and Table III.

V. Applications

In this section, applications are presented of PSEC calculating various axisymmetric tokamak plasma equilibria. Figures 8 to 13 show free-boundary equilibrium calculations while Figs. 14 and 15 give examples of fixed-boundary equilibria.

Figure 8a shows a Columbia University Torus II free-boundary equilibrium together with the vacuum flux contours. This is a high-beta (volume-averaged beta $\langle\beta\rangle = 10.8\,\%$) and highly elongated (2.235 to 1) plasma equilibrium with a plasma current of 18.57 kA and an aspect ratio of 4.85. The mid-plane safety factor (q) profile, current profile, pressure gradient ($dp/d\chi$) profile, and pressure profile are shown in Figs. 8b, 8c, 8d, and 8e, respectively. Spectral amplitude profiles for the ellipticity E, shift (x^{0c}), triangularity (x^{2c}), and squareness (x^{3c}) of the Torus II equilibrium are shown in Figs. 9a, 9b, 9c, and 9d, respectively. In Fig. 9e, the logarithm of the mean-square error, $\log \varepsilon$, and boundary squareness x_b^{3c} for the Torus II equilibrium are plotted versus the free-boundary iteration step to illustrate the convergence of the iteration scheme. For a high-beta equilibrium such as that in Torus II, the number of free-boundary iterations needed for convergence could be as high as 267, while for a low-beta equilibrium the number could be as low as 40 or 50. In Fig. 8 and all the other figures, the current density profile j is measured in units of $2\pi\mu_0/B_0$, i.e., the real current density $j_{\text{real}} = jB_0/2\pi\mu_0$ amperes/meter^2, the pressure profile p is measured in units of μ_0/B_0^2 ($p_{\text{real}} = pB_0^2/\mu_0$), and $p' = dp/d\chi$ is measured in units of $2\pi\mu_0/B_0$, i.e., $(dp/d\chi)_{\text{real}} = dp/d\chi\ B_0/2\pi\mu_0$ newtons/(meters^2 weber) with B_0 given in teslas.

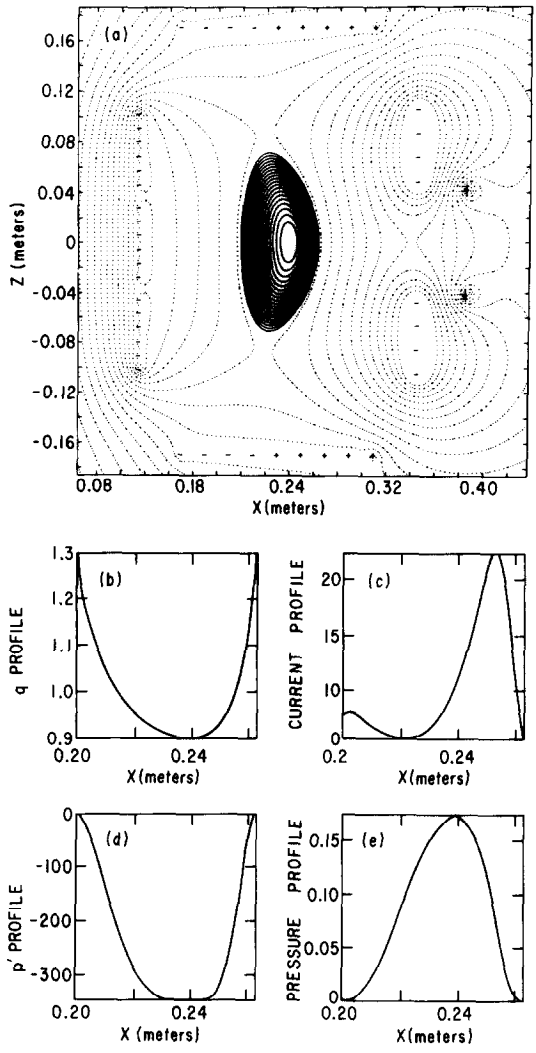

FIG. 8. (a) A Columbia University Torus II free-boundary equilibrium with $\langle\beta\rangle = 10.8\%$ and $I_p = 18.57$ kA; (b) to (e) are the mid-plane safety factor (q), current density (j), pressure gradient ($p' \equiv dp/d\chi$), and pressure (p) profiles.

An upgrade of Torus II has been designed, and Fig. 10a shows a typical free-boundary equilibrium with a plasma current of 14 kA, an average beta of 16.6%, and an aspect ratio of 5.3. The q profile, current profile, pressure gradient, and pressure profiles are shown in Figs. 10b to 10e, with the other parameters being given in Table IV. The stability of Torus II [10] and Torus II upgrade equilibria are being studied and will be reported elsewhere.

A TFTR (Tokamak Fusion Test Reactor) equilibrium with 1-MA plasma

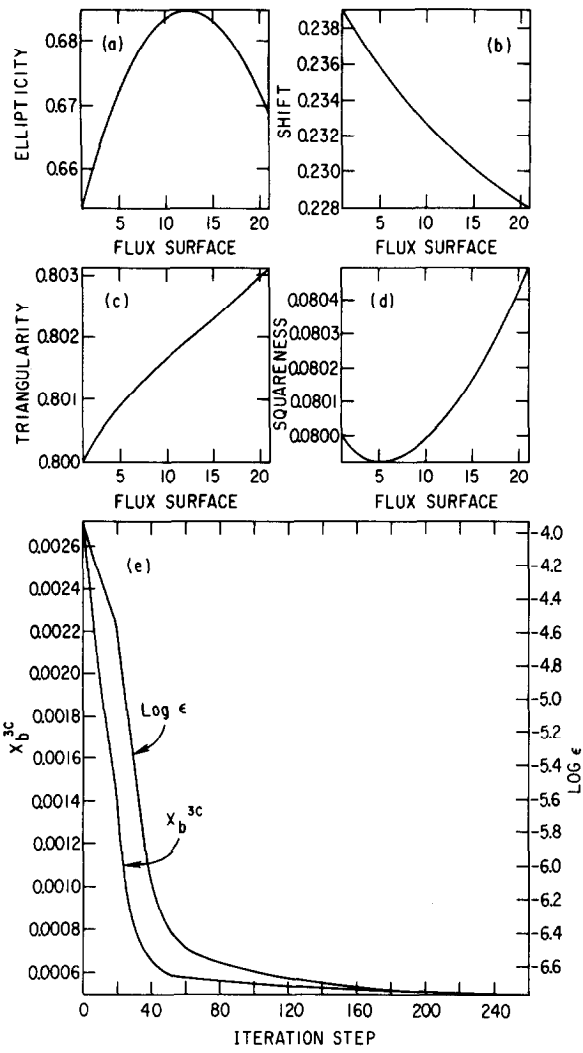

FIG. 9. The same equilibrium as that in Fig. 8; (a) to (d) are the ellipticity (E), shift (x^{0c}), triangularity (x^{2c}), and squareness (x^{3c}) profiles; (e) shows the convergence of the mean-square error ε and the boundary squareness (x_b^{3c}) as a function of the free-boundary iteration step.

current, an average beta of 4.7%, and a minor radius of 1 meter is shown in Fig. 11a. The plasma cross section is almost circular. The profiles of the equilibrium are shown in Figs. 11b to 11e while Table IV gives the other parameters. The positions of the coils have been given in Table III. In this run $I_{OH} = 9.5$ KA, $I_{EF} = 9.9$ KA, and $I_{VC} = -5$ KA.

A PDX (Poloidal Divertor Experiment) circular discharge with a 335-KA plasma current and an average beta of 2.6% is shown in Fig. 12. All the actual PDX coils

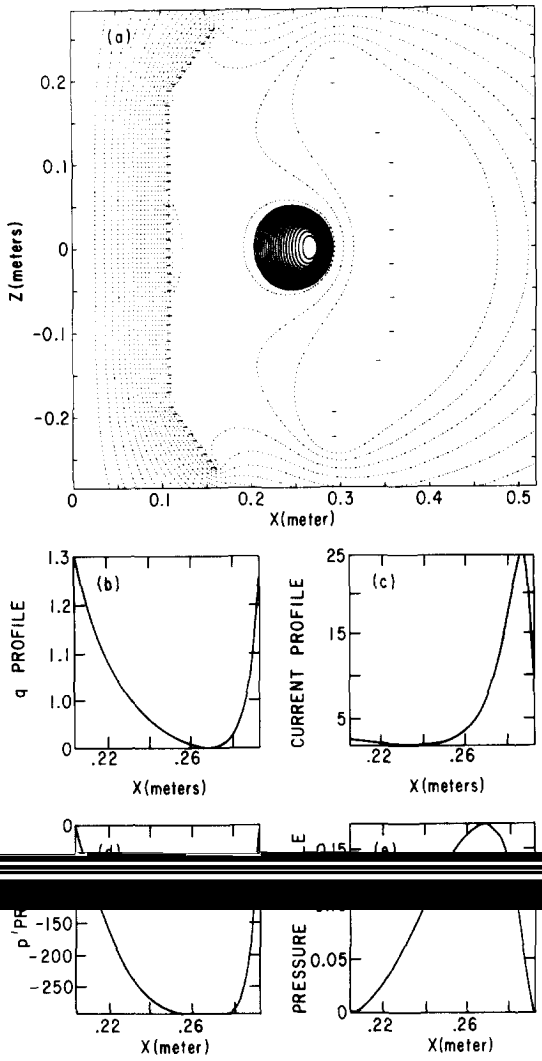

FIG. 10. (a) A free-boundary equilibrium of the Columbia University Torus II Upgrade with $\langle\beta\rangle = 16.6\%$ and $I_p = 14$ kA; (b) to (e) are the mid-plane safety factor (q), current density (j), pressure gradient ($p' \equiv dp/d\chi$), and pressure (p) profiles.

are included in the calculation. Other relevant parameters are given in Table IV. This calculation took five seconds on the Cray-1 computer.

So far all the free-boundary equilibria are up–down symmetric. PSEC can also calculate up–down asymmetric free-boundary equilibria. An example is shown in Fig. 13.

Finally, two examples of fixed-boundary equilibria are given. Figure 14a shows a

TABLE IV

Parameters for the Torus II Equilibrium in Fig. 8, the Torus II Upgrade Equilibrium in Fig. 10, the Free-Boundary TFTR Equilibrium in Fig. 11, and the Free-Boundary PDX Equilibrium in Fig. 12

	Torus II	Torus II Upgrade	TFTR	PDX
χ_0	−0.0011	−0.00095	−0.277	−0.0697
p_0	0.175	0.175	0.045	0.03722
$p_{\min}$	0.0	0.0	0.0	0.0
α_1	3.0	2	2	2
q_0	0.9	0.9	1.0	0.8
α_3	0.53	0.53	1.325	1.035
B_0 (kg)	3.3	3.3	15	9.597
R_0 (m)	0.225	0.225	2.5	1.4
$\sqrt{T}$ (m)	0.047	0.047	1.0	0.39
N_ψ	21	21	11	11
N_H	5	3	3	3
$\langle\beta\rangle$	10.8%	16.6%	4.7%	2.6%
I_p (kA)	18.57	14	1000.	335

high-beta equilibrium with an average beta of 19.6% while Figs. 14b to 14e give the various profiles. An up–down asymmetric equilibrium with an average beta of 7% is shown in Fig. 15a with the profiles shown in Figs. 15b to 15e.

VI. Summary

A new computer code, PSEC, has been developed to compute free-boundary toroidal plasma equilibria that are consistent with currents in external coils. The spectral variational technique used builds upon a recently published method for solving for interior plasma equilibrium once the shape of the plasma–vacuum interface is known. The attractive features of this code are its fast running speed, its versatility in being able to compute a wide variety of both low-β and high-β toroidal equilibrium, and its verified convergence properties. The quasilinearization method of solution allows the number of spectral harmonics included to be arbitrarily large, subject only to the limitation of computer memory size. This is in contrast to techniques previously described that utilize shooting methods that quickly become unwieldy as the number of harmonics becomes large.

Both up–down symmetric and asymmetric equilibria can be computed with the representation used here. Also, the special treatment of the center point leads to extremely accurate solutions near this singular point. A vindication of the representation employed lies in the code's demonstrated ability to compute fast, accurate equilibria.

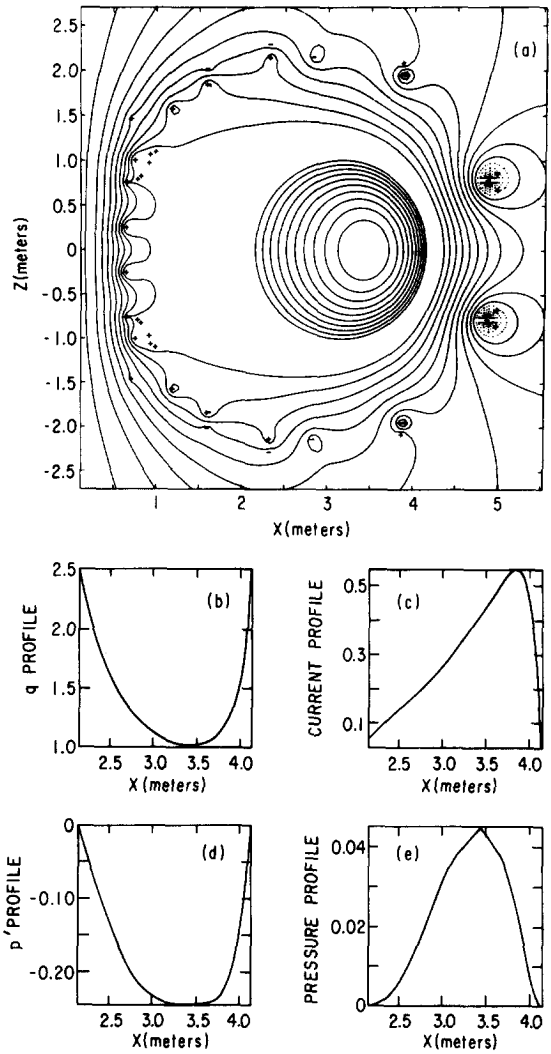

FIG. 11. (a) A TFTR free-boundary equilibrium with $I_p = 1$ MA, $\langle \beta \rangle = 4.7\%$, and minor radius $a = 1$ m; (b) to (e) show the mid-plane safety factor (q), current density (j), pressure gradient ($p' \equiv dp/d\chi$), and pressure (p) profiles.

The PSEC code is one of the PEST [11] family of computer programs in that it has the capability of writing equilibrium disk files that can be used by the PEST low-n stability or balloon codes for performing ideal and resistive MHD stability analyses. The speed and overstability of this code make it natural for use as the kernal of an evolution code which solves the time-dependent circuit equations for

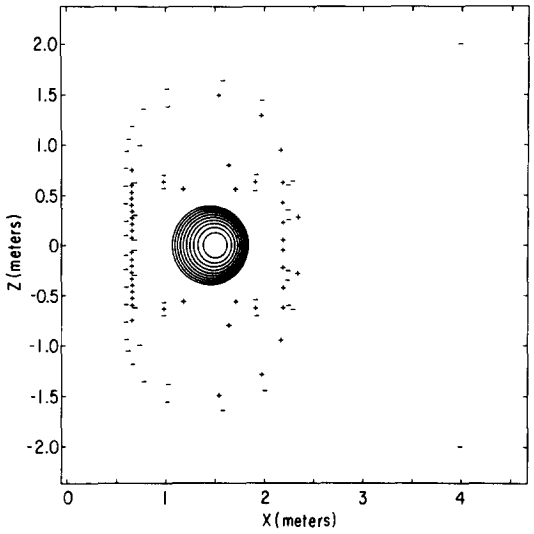

FIG. 12. A PDX circular discharge with all the PDX coils and $\langle\beta\rangle = 2.6\%$ and $I_p = 335$ kA.

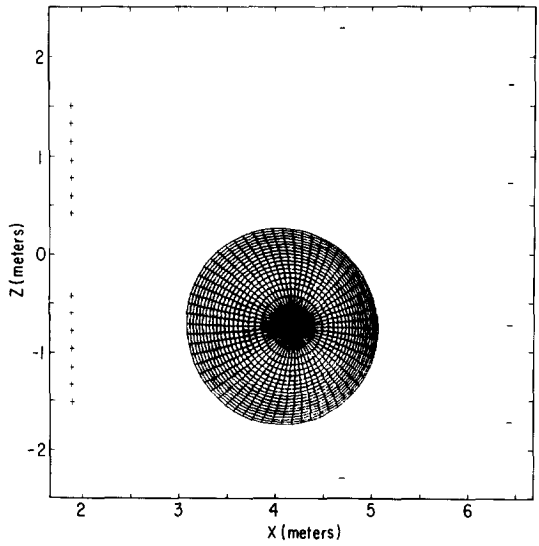

FIG. 13. A free-boundary up–down asymmetric equilibrium.

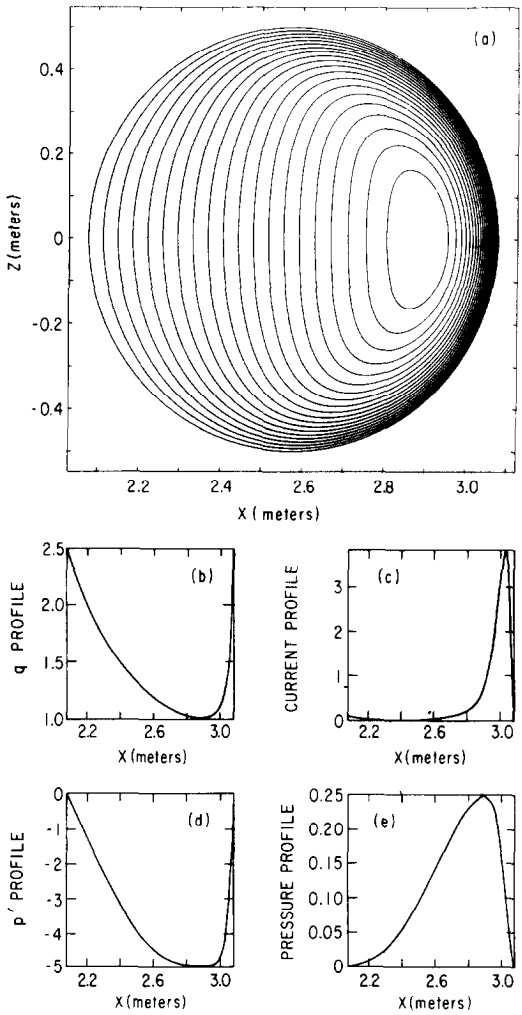

FIG. 14. (a) A high-β ($\langle\beta\rangle = 19.6\%$), fixed-boundary, up–down symmetric equilibrium; (b) to (e) give the mid-plane safety factor (q), current density (j), pressure gradient ($p' \equiv dp/d\chi$), and pressure (p) profiles.

external conducting coils to follow the evolution of axisymmetric modes in tokamaks on the resistive scale of the external conductors.

APPENDIX A

Here we specialize to the up–down symmetric case with $z_1^{0c} = z_1^{1c} = 0$ although in the code the general up–down asymmetric case is implemented. Then we have only two equations which give the derivative boundary conditions at the origin for E

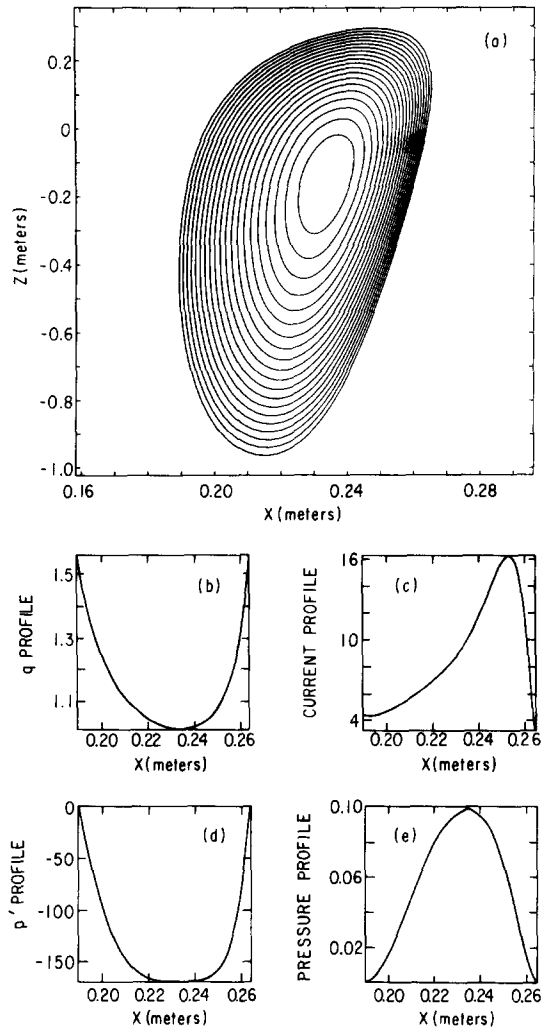

FIG. 15. (a) An up–down asymmetric, fixed-boundary equilibrium with $\langle\beta\rangle = 7\%$; (b) to (e) show the mid-plane safety factor (q), current density (j), pressure gradient ($p' \equiv dp/d\chi$), and pressure (p) profiles.

and x^{0c}. We assume a more general spectral representation for z than that in Eq. (13b) while x is still given by Eq. (13a):

$$z(\psi, \theta) = z^{0c}(\psi) + \sqrt{\psi T}\, E^{-1}(\psi) \sin\theta + \sqrt{\psi}\, z^{1c}(\psi) \cos\theta + \sum_{m=2}^{M} \psi^{(m-2)/2} [z^{mc}(\psi) \cos m\theta + z^{ms}(\psi) \sin m\theta]. \quad \text{(A.1)}$$

Equation (A.1) reduces to Eq. (13b) if

$$z^{mc}(\psi) = \sigma_{a,m} z^{ms}(\psi) \tag{A.2a}$$

and

$$z^{ms}(\psi) = \sigma_{s,m} x^{mc}(\psi) \tag{A.2b}$$

for $m = 2,..., M$. For the up–down symmetric case, $z^{0c} = z^{1c} = z^{mc} = x^{ms} = 0$, $m = 2,..., M$. Then we have

$$x_1^{0c} = \frac{1}{(1+3E_0^{-4})} \left\{ \frac{T}{2x_0} \left[\frac{Tx_0^2 P'(0)}{\chi_1} - E_0^{-2} \right] - 2E_0^2 z_1^{2s} + x_1^{2c}(1-3E_0^{-4}) \right\}, \tag{A.3}$$

and

$$\begin{aligned} 12(1+E_0^{-4})\, E_1 = {} & \frac{24}{TE_0^5} (x_1^{0c})^2 + \frac{2}{E_0 x_0} (E_0^2 + 4E_0^{-2})\, x_1^{0c} \\ & + \frac{2T}{x_0^2 E_0} - \frac{E_0 T^2}{2\chi_1} P'(0) - 4 \frac{\chi_2}{\chi_1} (E_0 - E_0^{-3}) \\ & - \frac{2z_1^{2s}}{E_0 x_0} \left[2(1-E_0^4) - E_0^2 x_0^2 TP'(0)/\chi_1 + 4 \frac{x_0 x_1^{0c}}{T} (2E_0^2 + 3E_0^{-2}) \right] \\ & + \frac{4}{T} (E_0^3 - 3E_0^{-1})(z_1^{2s})^2 - \frac{12}{TE_0} (1-3E_0^{-4})(x_1^{2c})^2 \\ & - \frac{2x_1^{2c}}{E_0 x_0} \left[E_0^2 - 5E_0^{-2} - 6 \frac{x_0 x_1^{0c}}{T} (1+5E_0^{-4}) \right] \\ & + 8 \frac{z_1^{2s} x_1^{2c}}{E_0 T} (3E_0^2 - E_0^{-2}) \\ & - 6 \frac{z_1^{3s}}{\sqrt{T}} (3E_0^2 - E_0^{-2}) \\ & + 6 \frac{x_1^{3c}}{\sqrt{T}} (1-3E_0^{-4}). \end{aligned} \tag{A.4}$$

Appendix B

The matrix elements of $\vec{A}$ in Eq. (21) are as follows:

$$A_{11} = 2\chi_\psi^2 \langle x^2 I_3 T_E^2 \rangle \sqrt{\psi T}$$

$$A_{12} = 2\chi_\psi^2 \langle x^2 I_3 T_E z_\theta \rangle$$

$$A_{13} = 2\chi_\psi^2 \langle x^2 I_3 T_E T_{2c} \rangle$$

$$A_{14} = 2\chi_\psi^2 \langle x^2 I_3 T_E T_{3c} \rangle \sqrt{\psi}$$

$$A_{15} = -2\chi_\psi^2 \langle x^2 I_3 T_E x_\theta \rangle$$

$$A_{16} = -2\chi_\psi^2 \langle x^2 I_3 T_E x_\theta \cos\theta \rangle \sqrt{\psi}$$

$$A_{17} = 2\chi_\psi^2 \langle x^2 I_3 T_E T_{2s} \rangle$$

$$A_{18} = 2\chi_\psi^2 \langle x^2 I_3 T_E T_{3s} \rangle \sqrt{\psi}$$

$$A_{21} = A_{12} \sqrt{\psi T}$$

$$A_{22} = 2\chi_\psi^2 \langle x^2 I_3 z_\theta^2 \rangle$$

$$A_{23} = 2\chi_\psi^2 \langle x^2 I_3 z_\theta T_{2c} \rangle$$

$$A_{24} = 2\chi_\psi^2 \langle x^2 I_3 z_\theta T_{3c} \rangle \sqrt{\psi}$$

$$A_{25} = -2\chi_\psi^2 \langle x^2 I_3 z_\theta x_\theta \rangle$$

$$A_{26} = -2\chi_\psi^2 \langle x^2 I_3 z_\theta x_\theta \cos\theta \rangle \sqrt{\psi}$$

$$A_{27} = 2\chi_\psi^2 \langle x^2 I_3 z_\theta T_{2s} \rangle$$

$$A_{28} = 2\chi_\psi^2 \langle x^2 I_3 z_\theta T_{3s} \rangle \sqrt{\psi}$$

$$A_{31} = A_{13} \sqrt{\psi T}$$

$$A_{32} = A_{23}$$

$$A_{33} = 2\chi_\psi^2 \langle x^2 I_3 T_{2c}^2 \rangle$$

$$A_{34} = 2\chi_\psi^2 \langle x^2 I_3 T_{2c} T_{3c} \rangle \sqrt{\psi}$$

$$A_{35} = -2\chi_\psi^2 \langle x^2 I_3 T_{2c} x_\theta \rangle$$

$$A_{36} = -2\chi_\psi^2 \langle x^2 I_3 T_{2c} x_\theta \cos\theta \rangle \sqrt{\psi}$$

$$A_{37} = 2\chi_\psi^2 \langle x^2 I_3 T_{2c} T_{2s} \rangle$$

$$A_{38} = 2\chi_\psi^2 \langle x^2 I_3 T_{2c} T_{3s} \rangle \sqrt{\psi}$$

$$A_{41} = A_{14} \sqrt{T}$$

$$A_{42} = A_{24} / \sqrt{\psi}$$

$$A_{43} = A_{34} / \sqrt{\psi}$$

$$A_{44} = 2\chi_\psi^2 \langle x^2 I_3 T_{3c}^2 \rangle \sqrt{\psi}$$

$$A_{45} = -2\chi_\psi^2 \langle x^2 I_3 T_{3c} x_\theta \rangle$$

$$A_{46} = -2\chi_\psi^2 \langle x^2 I_3 T_{3c} x_\theta \cos\theta \rangle \sqrt{\psi}$$

$$A_{47} = 2\chi_\psi^2 \langle x^2 I_3 T_{3c} T_{2s} \rangle$$

$$A_{48} = 2\chi_\psi^2 \langle x^2 I_3 T_{3c} T_{3s} \rangle \sqrt{\psi}$$

$$A_{51} = -\langle x^2 I_3 x_\theta T_E \rangle \sqrt{\psi T}$$

$$A_{52} = -\langle x^2 I_3 x_\theta z_\theta \rangle$$

$$A_{53} = -\langle x^2 I_3 x_\theta T_{2c} \rangle$$

$$A_{54} = -\langle x^2 I_3 x_\theta T_{3c} \rangle \sqrt{\psi}$$

$$A_{55} = \langle x^2 I_3 x_\theta^2 \rangle$$

$$A_{56} = \langle x^2 I_3 x_\theta^2 \cos\theta \rangle \sqrt{\psi}$$

$$A_{57} = -\langle x^2 I_3 x_\theta T_{2s} \rangle$$

$$A_{58} = -\langle x^2 I_3 x_\theta T_{3s} \rangle \sqrt{\psi}$$

$$A_{61} = A_{16} \sqrt{T}$$

$$A_{62} = A_{26}/\sqrt{\psi}$$

$$A_{63} = A_{36}/\sqrt{\psi}$$

$$A_{64} = A_{46}$$

$$A_{65} = 2\chi_\psi^2 \langle x^2 I_3 x_\theta^2 \cos\theta \rangle$$

$$A_{66} = 2\chi_\psi^2 \langle x^2 I_3 x_\theta^2 \cos^2\theta \rangle \sqrt{\psi}$$

$$A_{67} = -2\chi_\psi^2 \langle x^2 I_3 x_\theta T_{2s} \cos\theta \rangle$$

$$A_{68} = -2\chi_\psi^2 \langle x^2 I_3 x_\theta T_{3s} \cos\theta \rangle \sqrt{\psi}$$

$$A_{71} = A_{17} \sqrt{\psi T}$$

$$A_{72} = A_{27}$$

$$A_{73} = A_{37}$$

$$A_{74} = A_{47} \sqrt{\psi}$$

$$A_{75} = -2\chi_\psi^2 \langle x^2 I_3 T_{2s} x_\theta \rangle$$

$$A_{76} = A_{67} \sqrt{\psi}$$

$$A_{77} = 2\chi_\psi^2 \langle x^2 I_3 T_{2s}^2 \rangle$$

$$A_{78} = 2\chi_\psi^2 \langle x^2 I_3 T_{2s} T_{3s} \rangle \sqrt{\psi}$$

$$A_{81} = A_{18} \sqrt{T}$$

$$A_{82} = A_{28}/\sqrt{\psi}$$

$$A_{83} = A_{38}/\sqrt{\psi}$$

$$A_{84} = A_{48}$$

$$A_{85} = -2\chi_\psi^2 \langle x^2 I_3 T_{3s} x_\theta \rangle$$

$$A_{86} = A_{68}$$

$$A_{87} = A_{78}/\sqrt{\psi}$$

$$A_{88} = 2\chi_\psi^2 \langle x^2 I_3 T_{3s}^2 \rangle \sqrt{\psi}$$

where

$$I_3 \equiv (x_\theta^2 + z_\theta^2)/J^3, \tag{B.1}$$

$$T_E \equiv z_\theta \cos\theta + x_\theta E^{-2} \sin\theta, \tag{B.2}$$

$$T_{mc} \equiv z_\theta \cos m\theta - x_\theta \sigma_{s,m} \sin m\theta, \tag{B.3}$$

and

$$T_{ms} \equiv z_\theta \sin m\theta - x_\theta \sigma_{a,m} \cos m\theta, \tag{B.4}$$

for $m = 2, 3, 4, \ldots$.

The components of the vector $\vec{D}$ in Eq. (21) are:

$$\begin{aligned} D_1 = {} & \chi_\psi^2 \left\langle x \frac{\partial I_2}{\partial \theta} u_6 \right\rangle - 2\chi_\psi \left(p' \langle x T_E \rangle + R_0^2 g g' \left\langle \frac{T_E}{x} \right\rangle \right) \\ & - 2\chi_\psi \chi_{\psi\psi} \langle x T_E I_2 \rangle \\ & + 2\chi_\psi^2 \left\langle \frac{u_3}{J} - x T_E \frac{u_4}{J^2} + I_2 x_\psi T_E \right. \\ & \left. + x^2 T_E I_3 (\bar{x}_{\psi\psi} z_\theta - \bar{z}_{\psi\psi} x_\theta + u_5) \right\rangle, \end{aligned}$$

$$\begin{aligned} D_2 = {} & \chi_\psi^2 \left\langle x \frac{\partial I_2}{\partial \theta} z_\psi \right\rangle - 2\chi_\psi \left(p' \langle x z_\theta \rangle + R_0^2 g g' \left\langle \frac{z_\theta}{x} \right\rangle \right) \\ & - 2\chi_\psi \chi_{\psi\psi} \langle x I_2 z_\theta \rangle \\ & + 2\chi_\psi^2 \left\langle z_\theta \left(x_\psi I_2 - x \frac{u_4}{J^2} \right) \right. \\ & \left. + x^2 z_\theta I_3 (\bar{x}_{\psi\psi} z_\theta - \bar{z}_{\psi\psi} x_\theta + u_5) \right\rangle, \end{aligned}$$

$$\begin{aligned} D_3 = {} & \chi_\psi^2 \left\langle x \frac{\partial I_2}{\partial \theta} (z_\psi \cos 2\theta - \sigma_{s,2} x_\psi \sin 2\theta) \right\rangle \\ & - 2\chi_\psi \left(p' \langle x T_{2c} \rangle + R_0^2 g g' \left\langle \frac{T_{2c}}{x} \right\rangle \right) \\ & - 2\chi_\psi \chi_{\psi\psi} \langle x I_2 T_{2c} \rangle \end{aligned}$$

$$+2\chi_\psi^2\left\langle\frac{2}{J}(x_\theta\sin 2\theta-\sigma_{s,2}z_\theta\cos 2\theta)+T_{2c}\left(x_\psi I_2-\frac{xu_4}{J^2}\right)\right.$$

$$\left.+x^2T_{2c}I_3(\bar{x}_{\psi\psi}z_\theta-\bar{z}_{\psi\psi}x_\theta+u_5)\right\rangle,$$

$$D_4=\chi_\psi^2\left\langle x\frac{\partial I_2}{\partial\theta}(z_\psi\cos 3\theta-\sigma_{s,3}x_\psi\sin 3\theta)\right\rangle$$

$$-2\chi_\psi\left(p'\langle xT_{3c}\rangle+R_0^2gg'\left\langle\frac{T_{3c}}{x}\right\rangle\right)$$

$$-\chi_\psi\chi_{\psi\psi}\langle xI_2T_{3c}\rangle$$

$$+2\chi_\psi^2\left\langle\frac{3}{J}(x_\theta\sin 3\theta-\sigma_{s,3}z_\theta\cos 3\theta)+T_{3c}\left(x_\psi I_2-\frac{xu_4}{J^2}\right)\right.$$

$$\left.+x^2T_{3c}I_3(\bar{x}_{\psi\psi}z_\theta-\bar{z}_{\psi\psi}x_\theta+u_5)\right\rangle,$$

$$D_5=\left\langle\frac{xx_\theta u_4}{J^2}+I_2\frac{(xx_{\theta\psi}-x_\theta x_\psi)}{2}-x^2x_\theta I_3(\bar{x}_{\psi\psi}z_\theta-\bar{z}_{\psi\psi}x_\theta+u_5)\right\rangle,$$

$$D_6=-\chi_\psi^2\left\langle xx_\psi\cos\theta\frac{\partial I_2}{\partial\theta}\right\rangle+2\chi_\psi\left(p'\langle xx_\theta\cos\theta\rangle+R_0^2gg'\left\langle\frac{x_\theta\cos\theta}{x}\right\rangle\right)$$

$$+2\chi_\psi\chi_{\psi\psi}\langle xx_\theta I_2\cos\theta\rangle$$

$$+2\chi_\psi^2\left\langle\frac{z_\theta\sin\theta}{J}+\frac{xx_\theta u_4\cos\theta}{J^2}-I_2x_\theta x_\psi\cos\theta\right.$$

$$\left.-x^2x_\theta I_3\cos\theta(\bar{x}_{\psi\psi}z_\theta-\bar{z}_{\psi\psi}x_\theta+u_5)\right\rangle,$$

$$D_7=\chi_\psi^2\left\langle x\frac{\partial I_2}{\partial\theta}(z_\psi\sin 2\theta-\sigma_{a,2}x_\psi\cos 2\theta)\right\rangle$$

$$-2\chi_\psi\left(p'\langle xT_{2s}\rangle+R_0^2gg'\left\langle\frac{T_{2s}}{x}\right\rangle\right)$$

$$-2\chi_\psi\chi_{\psi\psi}\langle xI_2T_{2s}\rangle$$

$$+2\chi_\psi^2\left\langle\frac{-2}{J}(x_\theta\cos 2\theta-\sigma_{a,2}z_\theta\sin 2\theta)+T_{2s}\left(x_\psi I_2-\frac{xu_4}{J^2}\right)\right.$$

$$\left.+x^2T_{2s}I_3(\bar{x}_{\psi\psi}z_\theta-\bar{z}_{\psi\psi}x_\theta+u_5)\right\rangle,$$

$$D_8 = \chi_\psi^2 \left\langle x \frac{\partial I_2}{\partial \theta} (z_\psi \sin 3\theta - \sigma_{a,3} x_\psi \cos 3\theta) \right\rangle$$
$$- 2\chi_\psi \left(p' \langle x T_{3s} \rangle + R_0^2 g g' \left\langle \frac{T_{3s}}{x} \right\rangle \right)$$
$$- 2\chi_\psi \chi_{\psi\psi} \langle x I_2 T_{3s} \rangle$$
$$+ 2\chi_\psi^2 \left\langle - \frac{3}{J} (x_\theta \cos 3\theta - \sigma_{a,3} z_\theta \sin 3\theta) + T_{3s} \left(x_\psi I_2 - \frac{x u_4}{J^2} \right) \right.$$
$$\left. + x^2 T_{3s} I_3 (\bar{x}_{\psi\psi} z_\theta - \bar{z}_{\psi\psi} x_\theta + u_5) \right\rangle,$$

where

$$I_2 \equiv \frac{x_\theta^2 + z_\theta^2}{J^2}, \tag{B.5}$$

$$u_3 \equiv x_\theta \sin\theta + z_\theta E^{-2} \cos\theta, \tag{B.6}$$

$$u_4 \equiv x_\theta x_{\theta\psi} + z_\theta z_{\theta\psi}, \tag{B.7}$$

$$u_5 \equiv x_\psi z_{\theta\psi} - z_\psi x_{\theta\psi}, \tag{B.8}$$

$$u_6 \equiv x_\psi \cos\theta + x_\psi E^{-2} \sin\theta, \tag{B.9}$$

$\bar{x}_{\psi\psi}$ is the series for $x_{\psi\psi}$ with the $x_{\psi\psi}^{0c}$, $E_{\psi\psi}$, $x_{\psi\psi}^{2c}$, $x_{\psi\psi}^{3c}$, $x_{\psi\psi}^{2s}$, and $x_{\psi\psi}^{3s}$ terms absent; $\bar{z}_{\psi\psi}$ is the series for $z_{\psi\psi}$ with the $z_{\psi\psi}^{0c}$, $z_{\psi\psi}^{1c}$, $E_{\psi\psi}$, $x_{\psi\psi}^{2c}$, $x_{\psi\psi}^{3c}$, $x_{\psi\psi}^{2s}$, and $x_{\psi\psi}^{3s}$ terms absent; and T_{2c}, T_{3c} and T_{2s}, T_{3s} are given by Eq. (B.3) and Eq. (B.4), respectively, for $m = 2$ and 3.

Instead of the spectral amplitude vector $\vec{s}$ in Eq. (20b), we define a symmetric and an asymmetric spectral amplitude vector as follows:

$$\vec{s}^s = (x^{4c}, x^{5c}, \ldots, x^{Mc})^{\mathrm{T}},$$
$$\vec{s}^a = (x^{45}, x^{5s}, \ldots, x^{Ms})^{\mathrm{T}}.$$

Then from Eq. (22), we get

$$\vec{a}^s \cdot \vec{s}_{\psi\psi}^s + \vec{d}^s = 0,$$
$$\vec{a}^a \cdot \vec{s}_{\psi\psi}^a + \vec{d}^a = 0,$$

where $\vec{a}^s$ and $\vec{a}^a$ are $(M-3)\times(M-3)$ matrices, and $\vec{d}^s$ and $\vec{d}^a$ are $(M-3)\times 1$ vectors. We use a diagonal $\vec{a}^s$ and $\vec{a}^a$ whose elements are given by

$$a_{ii}^s = 2\chi_\psi^2 \psi^{(m-2)/2} \langle x^2 I_3 T_{mc}^2 \rangle,$$
$$a_{ii}^a = 2\chi_\psi^2 \psi^{(m-2)/2} \langle x^2 I_3 T_{ms}^2 \rangle,$$

where $i = 1,..., M-3$, $m = i+3$, I_3 is given by Eq. (B.1) and T_{mc} and T_{ms} are given in Eqs. (B.3) and (B.4). The components of $\vec{d}^s$ and $\vec{d}^a$ are:

$$
\begin{aligned}
d_i^s = \chi_\psi^2 & \left\langle x \frac{\partial I_2}{\partial \theta} (z_\psi \cos m\theta - \sigma_{s,m} x_\psi \sin m\theta) \right\rangle \\
& - 2\chi_\psi \left(p' \langle x T_{mc} \rangle + R_0^2 g g' \left\langle \frac{T_{mc}}{x} \right\rangle \right) \\
& - 2\chi_\psi \chi_{\psi\psi} \langle x T_{mc} I_2 \rangle \\
& + 2\chi_\psi^2 \left\langle \frac{m}{J} (x_\theta \sin m\theta - \sigma_{s,m} z_\theta \cos m\theta) + T_{mc} \left(x_\psi I_2 - \frac{x u_4}{J^2} \right) \right. \\
& \left. + x^2 T_{mc} I_3 (\bar{x}_{\psi\psi}^{mc} z_\theta - \bar{z}_{\psi\psi}^{mc} x_\theta + u_5) \right\rangle,
\end{aligned}
$$

$$
\begin{aligned}
d_i^a = \chi_\psi^2 & \left\langle x \frac{\partial I_2}{\partial \theta} (z_\psi \sin m\theta - \sigma_{a,m} x_\psi \cos m\theta) \right\rangle \\
& - 2\chi_\psi \left(p' \langle x T_{ms} \rangle + R_0^2 g g' \left\langle \frac{T_{ms}}{x} \right\rangle \right) \\
& - 2\chi_\psi \chi_{\psi\psi} \langle x T_{ms} I_2 \rangle \\
& + 2\chi_\psi^2 \left\langle - \frac{m}{J} (x_\theta \cos m\theta - \sigma_{a,m} z_\theta \sin m\theta) + T_{ms} \left(x_\psi I_2 - \frac{x u_4}{J^2} \right) \right. \\
& \left. + x^2 T_{ms} I_3 (\bar{x}_{\psi\psi}^{ms} z_\theta - \bar{z}_{\psi\psi}^{ms} x_\theta + u_5) \right\rangle,
\end{aligned}
$$

where $i = 1,..., M-3$, $m = i+3$, $\bar{x}_{\psi\psi}^{mc}$ and $\bar{z}_{\psi\psi}^{mc}$ are the series for $x_{\psi\psi}$ and $z_{\psi\psi}$ with the $x_{\psi\psi}^{mc}$ term absent, and $\bar{x}_{\psi\psi}^{ms}$ and $\bar{z}_{\psi\psi}^{ms}$ are the series for $x_{\psi\psi}$ and $z_{\psi\psi}$ with the term $x_{\psi\psi}^{ms}$ absent.

ACKNOWLEDGMENTS

It is a pleasure to acknowledge useful discussions with Dr. Morrell S. Chance, Dr. Donald A. Monticello, Dr. Francis W. Perkins, and Dr. Neil Pomphrey. This work was supported by U.S. Department of Energy Contract DE-AC02-CHO-3073.

REFERENCES

1. L. L. LAO, S. P. HIRSHMAN, AND R. M. WEILAND, *Phys. Fluids* **24** (1981), 1431.
2. K. M. LING AND S. C. JARDIN, *Bull. Amer. Phys. Soc.* **26** (1981), 957.
3. H. GRAD, *Phys. Fluids* **7** (1964), 1283.

4. M. D. KRUSKAL AND R. M. KULSRUD, *Phys. Fluids* **1** (1958), 265.
5. H. WEITZNER, Appendix of Ref. [1].
6. J. M. GREENE, J. L. JOHNSON, AND K. E. WEIMER, *Phys. Fluids* **14** (1971), 671.
7. S. C. JARDIN, Ph.D. thesis, pp. 128–129, Princeton University, 1976.
8. R. E. BELLMAN AND R. E. KALABA, "Quasilinearization and Nonlinear Boundary-Value Problems," Amer. Elsevier, New York, 1965.
9. G. DAHLQUIST AND ÅKE BJÖRCK, "Numerical Methods," pp. 438–439, Prentice–Hall, Englewood Cliffs, N.J., 1974.
10. F. M. LEVINTON, A. A. GROSSMAN, AND G. A. NAVRATIL, *Phys. Fluids* **27** (1984), 10.
11. R. C. GRIMM, J. M. GREENE, AND J. L. JOHNSON, *in* "Methods in Computational Physics" (J. Killeen, Ed.), Vol. 16, p. 253, Academic Press, New York, 1976.